γ-soft analog of the confined β-soft rotor model

Dennis Bonatsos* and D. Lenis†
Institute of Nuclear Physics, N.C.S.R. Demokritos, GR-15310 Aghia Paraskevi, Attiki, Greece

N. Pietralla‡
Institut für Kernphysik, Universität zu Köln, D-50937 Köln, Germany, and Institut für Kernphysik, Technische Universität Darmstadt, D-64289 Darmstadt, Germany

P. A. Terziev§
Institute for Nuclear Research and Nuclear Energy, Bulgarian Academy of Sciences, 72 Tzarigrad Road, BG-1784 Sofia, Bulgaria
(Received 8 May 2006; revised manuscript received 7 August 2006; published 13 October 2006)

A γ-soft analog of the confined β-soft rotor model is developed by using a γ-independent displaced infinite-well β potential in the Bohr Hamiltonian, for which exact separation of variables is possible. Level schemes interpolating between the E(5) critical point symmetry (with $R_{4/2} = E(4_1^+)/E(2_1^+) = 2.20$) and the O(5) γ-soft rotor (with $R_{4/2} = 2.50$) are obtained; these exhibit a crossover of excited 0^+ bandheads that lead to agreement with the general trends of 0_2^+ states in this region and is observed experimentally in ^{128,130}Xe.

DOI: 10.1103/PhysRevC.74.044306 PACS number(s): 21.60.Ev, 21.10.Re, 21.60.Fw, 27.60.+j

I. INTRODUCTION

Critical point symmetries [1,2], related to shape/phase transitions, have recently attracted considerable attention in the study of nuclear structure, since they provide parameter-free (up to overall scale factors) predictions supported by experimental evidence [3–6]. The E(5) critical point symmetry [1], in particular, is related to the shape/phase transition between vibrational [U(5)] and γ-unstable [O(6)] nuclei, whereas X(5) [2] is related to the transition between vibrational and axially symmetric prolate [SU(3)] nuclei. A systematic study of phase transitions in nuclear collective models has been given in [7–9].

In both the E(5) and X(5) models, exact [in E(5)] or approximate [in X(5)] separation of the β and γ collective variables of the Bohr Hamiltonian [10] is achieved, and an infinite square-well potential in β is used. (Various analytic solutions of the Bohr Hamiltonian have been recently reviewed in Ref. [11], and a recently introduced [12–14] computationally tractable version of the Bohr collective model is already in use [15].) Models interpolating between E(5) [or X(5)] and U(5) have been obtained by using β^{2n} potentials (with $n = 1, 2, 3, 4$) in the relevant [E(5) or X(5)] framework [16–18], whereas an interpolation between X(5) and the rigid rotor limit has been achieved in the framework of the confined β-soft (CBS) rotor model [19], by using in the X(5) framework infinite square-well potentials in β with boundaries $\beta_M > \beta_m \geqslant 0$, with the case of $\beta_m = 0$ corresponding to the original X(5) model. The CBS rotor model showed considerable success in describing transitional and strongly deformed nuclei in the rare earths and actinides [20,21].

In the present work an interpolation between E(5) and the γ-soft rotor [O(5)] limit is achieved by using in the E(5) framework γ-independent infinite square-well potentials in β with boundaries $\beta_M > \beta_m \geqslant 0$. The model contains one free parameter, $r_\beta = \beta_m/\beta_M$; the case with $r_\beta = 0$ corresponds to the original E(5) model, and $r_\beta \to 1$ leads to the γ-soft rotor [O(5)] limit. A special case with the two lowest excited 0^+ states being degenerate occurs for $r_{\beta_c} = 0.171$. Experimental examples on the E(5) side and on the O(5) side of r_{β_c} are found to correspond to ^{130}Xe and ^{128}Xe, respectively. The crossover of 0^+ bandheads observed at r_{β_c} is important in reproducing the experimental trends of 0_2^+ bandheads in the $R_{4/2} = E(4_1^+)/E(2_1^+)$ region between 2.20 [E(5)] and 2.50 [O(5)].

In Sec. II the calculation of the energy spectra and $B(E2)$ transition rates is described; results are shown and compared to experiment in Sec. III. An overall discussion of the present results in given in Sec. IV.

II. THE MODEL

We consider the Bohr Hamiltonian [10]

$$H = -\frac{\hbar^2}{2B}\left[\Delta_R + \frac{1}{\beta^2}\Delta_\Omega\right] + U(\beta), \tag{1}$$

with

$$\Delta_R = \frac{1}{\beta^4}\frac{\partial}{\partial\beta}\beta^4\frac{\partial}{\partial\beta} = \frac{\partial^2}{\partial\beta^2} + \frac{4}{\beta}\frac{\partial}{\partial\beta}, \tag{2}$$

$$\Delta_\Omega = \frac{1}{\sin 3\gamma}\frac{\partial}{\partial\gamma}\sin 3\gamma\frac{\partial}{\partial\gamma} - \sum_{k=1}^{3}\frac{L_k'^2(\theta_i)}{4\sin^2\left(\gamma - \frac{2\pi}{3}k\right)}, \tag{3}$$

where β and γ are the usual collective coordinates, L_k' ($k = 1, 2, 3$) are the components of angular momentum in the intrinsic frame, θ_i ($i = 1, 2, 3$) are the Euler angles, and B is

*Electronic address: bonat@inp.demokritos.gr
†Electronic address: lenis@inp.demokritos.gr
‡Electronic address: pietrall@ikp.uni-koeln.de
§Electronic address: terziev@inrne.bas.bg

the mass parameter. The potential $U(\beta)$ depends only on the collective coordinate β [22].

Using the factorized wave function $\Psi(\beta,\gamma,\theta_i) = F(\beta)\Phi(\gamma,\theta_i)$ [1,22] we can separate the Schrödinger equation corresponding to the Hamiltonian (1) into two parts:

(a) an angular part,

$$-\Delta_\Omega \Phi(\gamma,\theta_i) = \tau(\tau+3)\Phi(\gamma,\theta_i), \tag{4}$$

where τ is the seniority quantum number and Δ_Ω is a quadratic invariant operator of the group SO(5) [22,23] (for a detailed discussion see Ref. [23]), and

(b) a radial part,

$$\frac{d^2F(\beta)}{d\beta^2} + \frac{4}{\beta}\frac{dF(\beta)}{d\beta} + \left[\frac{2B}{\hbar^2}(E-U(\beta)) - \frac{\tau(\tau+3)}{\beta^2}\right] \times F(\beta) = 0. \tag{5}$$

In the radial equation (5) we consider an infinite-well potential [1,22] confined between boundaries [19] at β_m and β_M ($0 < \beta_m < \beta_M$):

$$U(\beta) = \begin{cases} 0, & \beta_m \leqslant \beta \leqslant \beta_M \\ \infty, & 0 \leqslant \beta < \beta_m, \quad \beta > \beta_M. \end{cases} \tag{6}$$

By defining $k^2 = 2BE/\hbar^2$ and substituting $F(\beta) = \beta^{-3/2}P(\beta)$, Eq. (5) in the interval $\beta \in [\beta_m, \beta_M]$ takes the form of a Bessel equation of νth order:

$$\beta^2 P''(\beta) + \beta P'(\beta) + (k^2\beta^2 - \nu^2)P(\beta) = 0, \tag{7}$$

where $\nu = \tau + 3/2$. The boundary conditions at β_m and β_M are

$$P(\beta_m) = 0, \qquad P(\beta_M) = 0, \qquad 0 < \beta_m < \beta_M. \tag{8}$$

The general solution of Eq. (7) is the cylindrical function

$$P(\beta) = aJ_\nu(k\beta) + bY_\nu(k\beta), \tag{9}$$

where $J_\nu(z)$ and $Y_\nu(z)$ are the Bessel functions of the first and second kind, respectively, of order $\nu = \tau + 3/2$, and (a, b) are constants to be determined. The boundary conditions (8) lead to a homogenous system for (a, b):

$$aJ_\nu(k\beta_M) + bY_\nu(k\beta_M) = 0,$$
$$aJ_\nu(k\beta_m) + bY_\nu(k\beta_m) = 0,$$

which has nontrivial solutions in (a, b) if its determinant is set to vanish:

$$J_\nu(k\beta_M)Y_\nu(k\beta_m) - J_\nu(k\beta_m)Y_\nu(k\beta_M) = 0. \tag{10}$$

In this way the boundary conditions (8) lead to a discrete spectrum of the parameter k, the values of which are the positive roots of Eq. (10). Equation (10) can be written in the form [19]

$$J_\nu(x)Y_\nu(r_\beta x) - J_\nu(r_\beta x)Y_\nu(x) = 0, \tag{11}$$

where $x = k\beta_M$ and the parameter r_β denotes the ratio $r_\beta = \beta_m/\beta_M$. Here we consider the case in which the parameter β_M is fixed and β_m varies in the range $0 < \beta_m < \beta_M$, the ratio r_β taking values in the interval $0 < r_\beta < 1$.

Let $x_{\xi\tau}^{(r_\beta)}$ be the ξth positive root of Eq. (11), and, respectively, $k_{\xi\tau}^{(r_\beta)} = x_{\xi\tau}^{(r_\beta)}/\beta_M$ be the ξth positive root of Eq. (10), where $\nu = \tau + 3/2$. Then the normalized eigenfunctions $P_{\xi\tau}^{(r_\beta)}(\beta)$ can be represented in the form

$$P_{\xi\tau}^{(r_\beta)}(\beta) = \left\lceil A_{\xi\tau}^{(r_\beta)}\right\rceil^{-1/2}\left\lceil J_\nu\left(k_{\xi\tau}^{(r_\beta)}\beta\right)Y_\nu\left(k_{\xi\tau}^{(r_\beta)}\beta_m\right) - J_\nu\left(k_{\xi\tau}^{(r_\beta)}\beta_m\right)Y_\nu\left(k_{\xi\tau}^{(r_\beta)}\beta\right)\right\rceil, \tag{12}$$

where $\beta_m \leqslant \beta \leqslant \beta_M$ and $k_{\xi\tau}^{(r_\beta)}\beta_m = r_\beta x_{\xi\tau}^{(r_\beta)}$. Then the normalized solutions of Eq. (5) in the interval $[\beta_m, \beta_M]$ are

$$F_{\xi\tau}^{(r_\beta)}(\beta) = \beta^{-3/2}P_{\xi\tau}^{(r_\beta)}(\beta). \tag{13}$$

The constants $A_{\xi\tau}^{(r_\beta)}$ in (12) are obtained from the normalization condition

$$\int_{\beta_m}^{\beta_M} \beta^4\left\lceil F_{\xi\tau}^{(r_\beta)}(\beta)\right\rceil^2 d\beta = \int_{\beta_m}^{\beta_M} \beta\left\lceil P_{\xi\tau}^{(r_\beta)}(\beta)\right\rceil^2 d\beta = 1. \tag{14}$$

The corresponding energy spectrum is

$$E_{\xi\tau}(r_\beta) = \frac{\hbar^2}{2B}\left[k_{\xi\tau}^{(r_\beta)}\right]^2 = \frac{\hbar^2}{2B\beta_M^2}\left[x_{\xi\tau}^{(r_\beta)}\right]^2. \tag{15}$$

In the limiting case of $\beta_m \to 0$ (or $r_\beta \to 0$) the spectrum and eigenfunctions correspond to the E(5) critical point symmetry [1].

The factorized wave functions are denoted by

$$|r_\beta;\xi\tau\mu LM\rangle \equiv \Psi_{\xi\tau\mu LM}^{(r_\beta)}(\beta,\gamma,\theta_i) = F_{\xi\tau}^{(r_\beta)}(\beta)\Phi_{LM}^{\tau\mu}(\gamma,\theta_i), \tag{16}$$

where τ is the seniority quantum number, $\mu = 0, 1, 2, \ldots, [\tau/3]$, and for a given value of μ the angular momentum L takes values $L = 2\rho, 2\rho-2, 2\rho-3, \ldots, \rho+1, \rho$, where $\rho = \tau - 3\mu$. The angular part of the wave function has the form [24]

$$\Phi_{LM}^{\tau\mu}(\gamma,\theta_i) = N_{\tau\mu L}^{-1/2}\sqrt{\frac{2L+1}{8\pi^2}}\sum_K \phi_{LK}^{\tau\mu}(\gamma)D_{MK}^{L*}(\theta_i), \tag{17}$$

where $N_{\tau\mu L}$ is a normalization constant and the index K in the sum takes even values in the interval $|K| \leqslant L$. In the present case we consider only states that are nondegenerate with respect to the quantum number L in the framework of the group embedding SO(5) $\supset$ SO(3).

The reduced transition probabilities $B(E2)$ for the $E2$ transitions,

$$B(E2;\alpha_i L_i \to \alpha_f L_f) = \frac{|\langle\alpha_f L_f\|T^{(E2)}\|\alpha_i L_i\rangle|^2}{2L_i+1}, \tag{18}$$

are calculated for the quadrupole operator $T^{(E2)}$ proportional to the collective variable α_m:

$$T_m^{(E2)} \propto \beta\left\{D_{m0}^{2*}(\theta_i)\cos\gamma + \frac{1}{\sqrt{2}}\left[D_{m2}^{2*}(\theta_i) + D_{m-2}^{2*}(\theta_i)\right]\sin\gamma\right\}. \tag{19}$$

As a result for the $E2$ transitions one has

$$B(E2;L_{\xi\tau\mu} \to L'_{\xi'\tau'\mu'}) = R^2_{\xi'\tau';\xi\tau}(r_\beta)\,G^2_{\tau'\mu'L';\tau\mu L}, \tag{20}$$

where

$$R_{\xi'\tau';\xi\tau}(r_\beta) = \int_{\beta_m}^{\beta_M} \beta F^{(r_\beta)}_{\xi'\tau'}(\beta) F^{(r_\beta)}_{\xi\tau}(\beta)\, \beta^4 d\beta, \qquad (21)$$

and $G_{\tau'\mu'L';\tau\mu L}$ are geometrical factors corresponding to the embedding SO(5) $\supset$ SO(3). The selection rules for the matrix elements of the quadrupole operator $T^{(E2)}_m$ defined in (19) are $|\Delta\tau| = 1$ and $|\Delta L| \leqslant 2$. We stress that all wave functions, energy eigenvalues, and transition matrix elements are exact analytical solutions of the Bohr Hamiltonian for the class of potentials considered here.

III. ANALYTICAL RESULTS AND COMPARISON TO EXPERIMENT

Analytical results for energy levels and $B(E2)$ transition rates are shown in Fig. 1. The main observation regards the position of the lowest excited 0^+ states. In E(5) [1] and for low values of $r_\beta < r_{\beta_c} = 0.171$, 0^+_2 corresponds to ($\xi = 2, \tau = 0$),

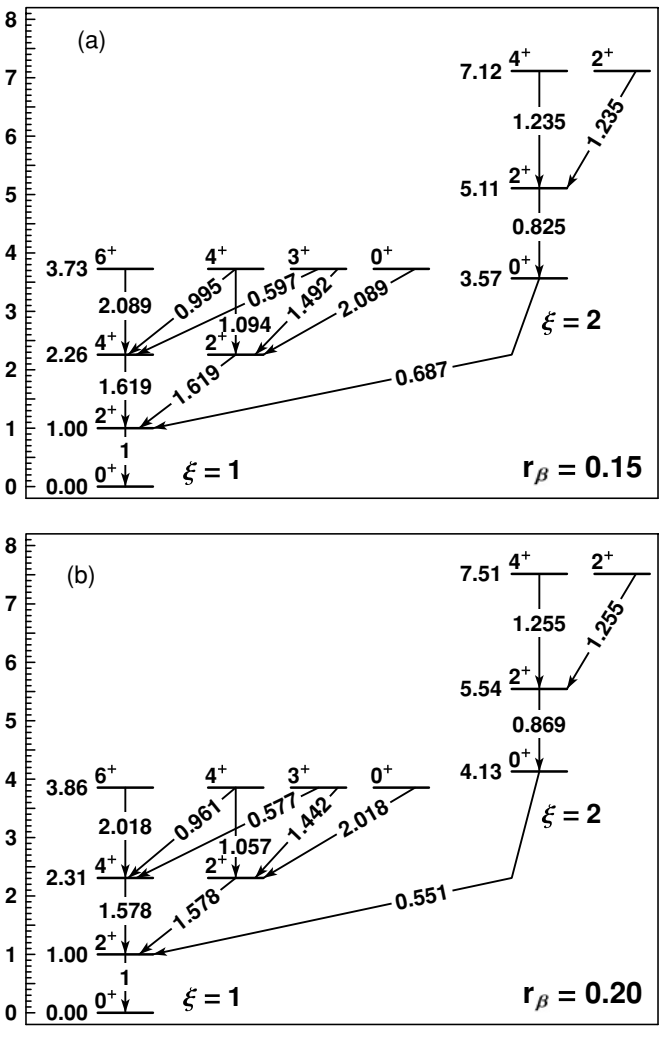

FIG. 1. Energy levels (normalized to the excitation energy of the 2^+_1 state) and $B(E2)$ transition rates [normalized to $B(E2; 2^+_1 \to 0^+_1)$] for two different values of the structural parameter $r_\beta = \beta_m/\beta_M$ around the $0^+_{2,3}$ crossing.

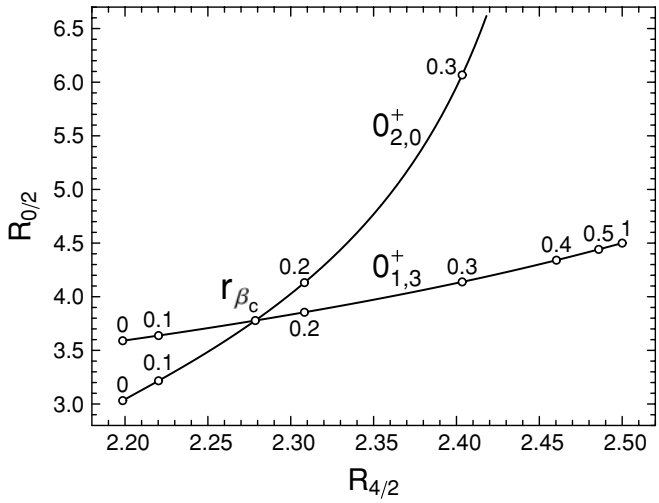

FIG. 2. Energy of 0^+ states (normalized to the energy of the 2^+_1 state), labeled as $R_{0/2}$, vs the ratio $R_{4/2} = E(4^+_1)/E(2^+_1)$. The parameter r_β on each curve starts from zero at the left end, increasing to the right. The crossover of the ($\xi = 2, \tau = 0, L = 0$) and the ($\xi = 1, \tau = 3, L = 0$) curves occurs at $r_{\beta_c} \approx 0.171263$, $(R_{4/2}, R_{0/2})_c \approx (2.27861, 3.77797)$.

whereas 0^+_3 is provided by ($\xi = 1, \tau = 3$). For higher values of $r_\beta > r_{\beta_c} = 0.171$ the picture is the opposite, with 0^+_2 corresponding to ($\xi = 1, \tau = 3$), and 0^+_3 given by ($\xi = 2, \tau = 0$). The latter eigenstate is shifted toward infinite energy as the O(5) limit is approached for $r_\beta \to 1$. The normalized 0^+ bandheads are shown as a function of the $R_{4/2} = E(4^+_1)/E(2^+_1)$ ratio in Fig. 2. On each curve the parameter r_β starts from $r_\beta = 0$ on the left, gradually increasing to the right. The crossover of the ($\xi = 2, \tau = 0$) and the ($\xi = 1, \tau = 3$) curves occurs at $r_{\beta_c} = 0.171$.

The existence of the 0^+ state's crossover is crucial in keeping the model predictions in agreement with the general trends shown by the experimental $R_{0/2} = E(0^+_2)/E(2^+_1)$ ratio as a function of the $R_{4/2} = E(4^+_1)/E(2^+_1)$ ratio, given in Ref. [25]. In the region with $2.20 < R_{4/2} < 2.50$, covered by the present model, the experimental $R_{0/2}$ values indeed stay below 5.0, in agreement with what is seen in Fig. 2 for the ($\xi = 1, \tau = 3$) bandhead.

It is interesting to identify nuclei corresponding to parameter values near the region $r_\beta = 0.15$–0.20, in which the crossover of the 0^+ bandheads occurs. Below $r_{\beta_c} = 0.171$ the situation resembles the one in E(5), with 6^+_1, 4^+_2, and 0^+_3 states being nearly degenerate, whereas the 0^+_2 state lies lower. Beyond $r_{\beta_c} = 0.171$ the near degeneracy applies to the 6^+_1, 4^+_2, and 0^+_2 states, whereas the 0^+_3 state lies higher. This situation occurs in the neighboring nuclei ^{130}Xe (corresponding to $r_\beta = 0.12$) and ^{128}Xe (reproduced by $r_\beta = 0.21$), shown in Fig. 3. (The parameter r_β has been fitted to the experimental $R_{4/2}$ ratio of each nucleus.) In the latter case, known $B(E2)$ values, too, agree remarkably well with the theoretical predictions.

Both before and after the crossover, the 0^+ bandhead with ($\xi = 1, \tau = 3$) is connected by a strong $E2$ transition to the 2^+_2 state, whereas the 0^+ bandhead with ($\xi = 2, \tau = 0$) decays less strongly to the 2^+_1 level. These interband $B(E2)$ values

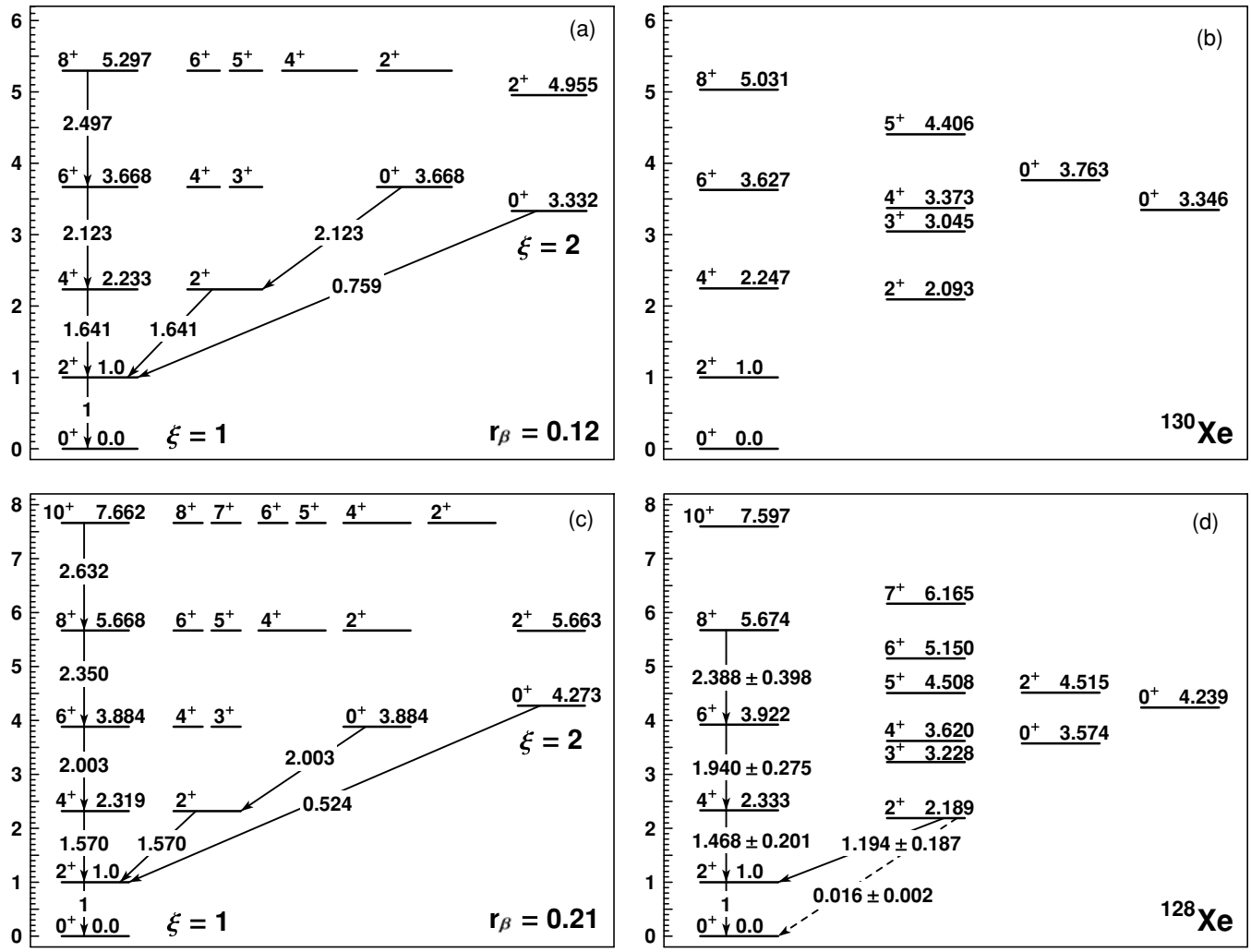

FIG. 3. Comparison of the model predictions for $r_\beta = 0.12$ (a) to the experimental data of ^{130}Xe [26] (b), and of the model predictions for $r_\beta = 0.21$ (c) to the experimental data for ^{128}Xe [27] (d).

provide a stringent test to the model. However, their absolute values are unknown experimentally.

It is nevertheless possible to unambiguously characterize the predominant nature of the two excited $0^+_{2,3}$ states of ^{128,130}Xe by considering their $E2$ decay branching ratios to the lowest two $2^+_{1,2}$ states. We thus define the double-ratio

$$\mathcal{Z}(0^+_{3/2}) = \frac{B(E2;0^+_3 \to 2^+_2)/B(E2;0^+_3 \to 2^+_1)}{B(E2;0^+_2 \to 2^+_2)/B(E2;0^+_2 \to 2^+_1)} \quad (22)$$

$$= \frac{\left(\frac{E_\gamma(0^+_3\to 2^+_1)}{E_\gamma(0^+_3\to 2^+_2)}\right)^5 \frac{I_\gamma(0^+_3\to 2^+_2)}{I_\gamma(0^+_3\to 2^+_1)}}{\left(\frac{E_\gamma(0^+_2\to 2^+_1)}{E_\gamma(0^+_2\to 2^+_2)}\right)^5 \frac{I_\gamma(0^+_2\to 2^+_2)}{I_\gamma(0^+_2\to 2^+_1)}} \quad (23)$$

for which one expects values >1 for $r_\beta < r_{\beta_c}$ and <1 for $r_\beta > r_{\beta_c}$, respectively. Equation (23) involves γ-ray energies and intensity ratios. The data [26–28] yield values of $\mathcal{Z}(0^+_{3/2}) = 52 \pm 30$ for ^{130}Xe and $\mathcal{Z}(0^+_{3/2}) = 0.32 \pm 0.17$ for ^{128}Xe, as given in Table I. The experimental values for ^{130}Xe and ^{128}Xe differ by two orders of magnitude. Despite the large uncertainties that originate in the 50% uncertainty for the low intensity of the initially forbidden $0^+ \to 2^+_2$ low-energy transition [26–28], the data prove the crossing of the different 0^+ configurations with $(\xi = 2, \tau = 0)$ and $(\xi = 1, \tau = 3)$ between ^{130}Xe and ^{128}Xe, as predicted by the model from a fit to the relative 4^+_1 excitation energy $R_{4/2}$.

Having identified the 0^+ configuration crossing we can analyze it quantitatively in a two-state mixing scenario. These close-lying experimental 0^+ states are considered as

TABLE I. Comparison of data [26–28] on ^{130,128}Xe to the model [O(5)-CBS] and the two-state mixing scenario (see Sec. III).

	^{130}Xe	O(5)-CBS $r_\beta = 0.12$	^{128}Xe	O(5)-CBS $r_\beta = 0.21$
$\mathcal{Z}(0^+_{3/2})$	52(30)	∞	0.32(17)	0
α^2_2	0.88(3)	–	0.43(3)	–
$\frac{B(E2;0^+_{1,3}\to 2^+_2)}{B(E2;0^+_{2,0}\to 2^+_1)}$	28(9)	2.8	3.7(1.0)	3.8

an orthogonal mixture of the crossing model states $0_2^+ = \alpha_2 0^+_{\xi=2,\tau=0} + \alpha_3 0^+_{\xi=1,\tau=3}$ and $0_3^+ = -\alpha_3 0^+_{2,0} + \alpha_2 0^+_{1,3}$ owing to residual interactions not accounted for by the simple model. This yields $\mathcal{Z}(0^+_{3/2}) = (\alpha_2/\alpha_3)^4$ owing to the τ-selection rules for the $E2$ operator in the unperturbed situation and allows the mixing coefficients to be determined. The squared amplitudes α_2^2 quantify the 0^+ configuration crossing. The contribution of the $0^+_{\xi=2,\tau=0}$ model state to the observed 0_2^+ state drops from 88(3)% in ^{130}Xe to 43(3)% in ^{128}Xe, as displayed in Table I.

With this information a further test of the model prediction for $E2$ transition rates can be performed by assuming only the validity of the two-state-mixing scenario. The relative strengths of the unperturbed interband $E2$ transitions can be extracted from the experimental $E2$ branching ratios

$$\left[\frac{B(E2;0^+_{1,3}\to 2^+_2)}{B(E2;0^+_{2,0}\to 2^+_1)}\right]_{\text{unperturbed}} = \left(\frac{\alpha_3}{\alpha_2}\right)^2 \left[\frac{B(E2;0^+_3\to 2^+_2)}{B(E2;0^+_3\to 2^+_1)}\right]_{\text{expt}} = \sqrt{\frac{\frac{I_\gamma(0^+_2\to 2^+_2)}{I_\gamma(0^+_2\to 2^+_1)}\left(\frac{E_\gamma(0^+_2\to 2^+_1)}{E_\gamma(0^+_2\to 2^+_2)}\right)^5}{\frac{I_\gamma(0^+_3\to 2^+_1)}{I_\gamma(0^+_3\to 2^+_2)}\left(\frac{E_\gamma(0^+_3\to 2^+_2)}{E_\gamma(0^+_3\to 2^+_1)}\right)^5}}\,. \tag{24}$$

The right-hand side (rhs) involves $E2$ intensity ratios in the perturbed (experimental) situation. The experimental values (rhs) are compared to the theoretical values for the left-hand side of Eq. (24) at the bottom of Table I. The data on ^{128}Xe coincide with the model within the uncertainties. The data on ^{130}Xe also exhibit the predicted dominance of the $B(E2;0^+_{1,3}\to 2^+_2)$ value over the $B(E2;0^+_{2,0}\to 2^+_2)$ value but by an order of magnitude more pronounced than theoretically expected. This numerical deviation calls for better data on the weak $0_2^+ \to 2_2^+$ 672-keV decay intensity with its present uncertainty of 50% [28].

IV. SUMMARY

A γ-soft analog of the confined β-soft rotor model has been constructed and exactly solved analytically by using a γ-independent displaced infinite-well β potential in the Bohr equation, in which exact separation of variables is possible in this case. The model obtained contains one free parameter, the ratio $r_\beta = \beta_m/\beta_M$ of the positions of the left wall (β_m) and the right wall (β_M) of the potential well, and interpolates between the E(5) critical point symmetry, possessing $R_{4/2} = E(4_1^+)/E(2_1^+) = 2.20$ and obtained for $r_\beta = 0$, and the γ-soft rotor O(5), having $R_{4/2} = 2.50$ and obtained for $r_\beta \to 1$. Owing to the explicit O(5) symmetry the model might be addressed as the *O(5)-confined β-soft rotor model* [O(5)-CBS]. A crossover of excited 0^+ bandheads as a function of $R_{4/2}$ is predicted, which is crucial in keeping the model predictions for the 0_2^+ bandhead in good agreement with experimental systematics in this region of $R_{4/2}$ ratios. This crossover is manifested in ^{128,130}Xe, as is seen quantitatively from experimental $E2$ decay intensity ratios. Information on relative and absolute $E2$ transitions in ^{128}Xe are in good agreement with the model predictions when simple configuration mixing is accounted for, whereas more accurate experimental information on $B(E2)'$s in ^{130}Xe is desirable for further significant tests of the model.

[1] F. Iachello, Phys. Rev. Lett. **85**, 3580 (2000).
[2] F. Iachello, Phys. Rev. Lett. **87**, 052502 (2001).
[3] R. F. Casten and N. V. Zamfir, Phys. Rev. Lett. **85**, 3584 (2000).
[4] R. F. Casten and N. V. Zamfir, Phys. Rev. Lett. **87**, 052503 (2001).
[5] R. M. Clark, M. Cromaz, M. A. Deleplanque, M. Descovich, R. M. Diamond, P. Fallon, I. Y. Lee, A. O. Macchiavelli, H. Mahmud, E. Rodriguez-Vieitez, F. S. Stephens, and D. Ward, Phys. Rev. C **69**, 064322 (2004).
[6] R. M. Clark, M. Cromaz, M. A. Deleplanque, M. Descovich, R. M. Diamond, P. Fallon, R. B. Firestone, I. Y. Lee, A. O. Macchiavelli, H. Mahmud, E. Rodriguez-Vieitez, F. S. Stephens, and D. Ward, Phys. Rev. C **68**, 037301 (2003).
[7] D. J. Rowe, Nucl. Phys. **A745**, 47 (2004).
[8] P. S. Turner and D. J. Rowe, Nucl. Phys. **A756**, 333 (2005).
[9] G. Rosensteel and D. J. Rowe, Nucl. Phys. **A759**, 92 (2005).
[10] A. Bohr, Mat. Fys. Medd. K. Dan. Vidensk. Selsk. **26**, 14 (1952).
[11] L. Fortunato, Eur. Phys. J. A **26**, **s01**, 1 (2005).
[12] D. J. Rowe, Nucl. Phys. **A735**, 372 (2004).
[13] D. J. Rowe, P. S. Turner, and J. Repka, J. Math. Phys. **45**, 2761 (2004).
[14] D. J. Rowe and P. S. Turner, Nucl. Phys. **A753**, 94 (2005).
[15] M. A. Caprio, Phys. Rev. C **72**, 054323 (2005).
[16] J. M. Arias, C. E. Alonso, A. Vitturi, J. E. García-Ramos, J. Dukelsky, and A. Frank, Phys. Rev. C **68**, 041302(R) (2003).
[17] D. Bonatsos, D. Lenis, N. Minkov, P. P. Raychev, and P. A. Terziev, Phys. Rev. C **69**, 044316 (2004).
[18] D. Bonatsos, D. Lenis, N. Minkov, P. P. Raychev, and P. A. Terziev, Phys. Rev. C **69**, 014302 (2004).
[19] N. Pietralla and O. M. Gorbachenko, Phys. Rev. C **70**, 011304(R) (2004).
[20] K. Dusling and N. Pietralla, Phys. Rev. C **72**, 011303(R) (2005).
[21] K. Dusling, N. Pietralla, G. Rainovski, T. Ahn, B. Bochev, A. Costin, T. Koike, T. C. Li, A. Linnemann, S. Pontillo, and C. Vaman, Phys. Rev. C **73**, 014317 (2006).
[22] L. Wilets and M. Jean, Phys. Rev. **102**, 788 (1956).
[23] D. R. Bès, Nucl. Phys. **10**, 373 (1959).
[24] E. Chacón and M. Moshinsky, J. Math. Phys. **18**, 870 (1977).
[25] W.-T. Chou, G. Cata-Danil, N. V. Zamfir, R. F. Casten, and N. Pietralla, Phys. Rev. C **64**, 057301 (2001).
[26] B. Singh, Nucl. Data Sheets **93**, 33 (2001).
[27] M. Kanbe and K. Kitao, Nucl. Data Sheets **94**, 227 (2001).
[28] H. Miyahara, H. Matumoto, G. Wurdiyanto, K. Yanagida, Y. Takenaka, A. Yoshida, and C. Mori, Nucl. Instrum. Methods A **353**, 229 (1994).